ACS OMEGA

http://pubs.acs.org/journal/acsodf

Article

Insight into the Technical Qualification of the Sonocogreen CaO/Clinoptilolite Nanocomposite ($CaO_{(NP)}$/Clino) as an Advanced Delivery System for 5-Fluorouracil: Equilibrium and Cytotoxicity

Mostafa R. Abukhadra,* Alyaa Adlii, Jong Seong Khim, Jamaan S. Ajarem, and Ahmed A. Allam

Cite This: *ACS Omega* 2021, 6, 31982−31992

Read Online

ACCESS | Metrics & More | Article Recommendations | Supporting Information

ABSTRACT: Clinoptilolite as a natural zeolite was integrated with green CaO nanoparticles forming the green nanocomposite $CaO_{(NP)}$/Clino. The $CaO_{(NP)}$/Clino composite was assessed as a potential carrier for 5-fluorouracil (5-FL) drug. The $CaO_{(NP)}$/Clino carrier achieved an enhanced 5-FL loading capacity of 305.3 mg/g as compared to 163 mg/g for pure clinoptilolite. The kinetics of the 5-FL loading follow the properties of the pseudo-first-order model, while the equilibrium results are related to the Langmuir isotherm. Therefore, the 5-FL loading processes occurred in the monolayer formed by homogeneous active loading receptors on the surface of the $CaO_{(NP)}$/Clino carrier. The Gaussian energy of the 5-FL loading reaction (9.2 KJ/mol) reflected the dominant effect for the chemical mechanisms, especially the zeolitic ion-exchange mechanisms. Additionally, the thermodynamic parameters suggested endothermic, feasible, and spontaneous properties for the occurred 5-FL loading reactions. The release profile of 5-FL from $CaO_{(NP)}$/Clino has continuous and long properties (150 h) at pH 1.2 (gastric fluid) and pH 7.4 (intestinal fluid). The kinetic studies of the release reactions show considerable agreement with Higuchi, Hixson−Crowell, and Korsmeyer−Peppas models. Such high fitting results and the diffusion exponent values (0.49 at pH 1.2 and 0.48 at pH 7.4) reflected the release properties of the Fickian transport behavior involving complex erosion and diffusion mechanisms. The cytotoxicity study of $CaO_{(NP)}$/Clino on colorectal normal cells (CCD-18Co) declare the safe and biocompatible effect as a carrier for the 5-FL drug. Additionally, $CaO_{(NP)}$/Clino as a carrier causes considerable enhancement for the cytotoxic effect of the loaded 5-FL drug on colon cancer cells (HCT-116).

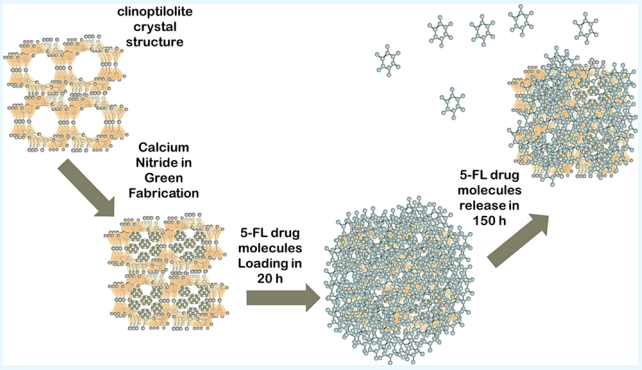

1. INTRODUCTION

Colorectal cancer is one of the widely distributed cancer species in the contemporary world and the essential reason for death especially in developing countries.[1,2] Moreover, the continuous growth in the number of patients demonstrates the predicted increase in their numbers by 75% within about 2 years.[3] Cancer chemotherapies were applied effectively in the treatment of cancer cells including several drugs such as the 5-fluorouracil (5-FL) drug.[4−6] The 5-FL drug is a common and very effective chemotherapy used in the treatment of different types of cancers including pancreas cancer, rectum cancer, stomach cancer, breast cancer, and colon cancer.[7] However, its application is associated with some observable technical and health drawbacks. It shows of cytotoxic effect, and its poor selectivity property shows toxic effects on normal cells and other organisms, especially if it is used at high dosages.[1,8] Additionally, the drug has low-solubility properties and a very fast diffusion rate, which causes a significant increase in the required dosages.[3,9,10]

Therefore, synthetic carriers and delivery systems with significant chemical and structural properties were assessed to avoid the reported side effects of the 5-FL drug and to enhance its therapeutic effect.[11] Synthetic carriers are used essentially to deliver the loaded 5-FL drug at managed dosage, systematic diffusion rate, aggressively pursued, and targeted pathways.[11,12] The introduced carriers in the later periods show considerable effects on (1) inducing the solubility of the 5-FL drug, (2) controlling its diffusion rate, (3) inducing its selectivity properties toward the target cells, (4) declining its degradation rate, (5) promoting the patient compliance, (6) keeping its concentration at the required therapeutic value, and (7) inducing the pharmacological and curative profiles.[4,13−15] The materials introduced as carriers for 5-FL drugs in the recent periods included biodegradable polymers,[16] kaolinite and

Received: August 31, 2021
Accepted: November 3, 2021
Published: November 17, 2021

halloysite,[3,10] zeolite,[17] MCM-based materials,[11] clay-based minerals,[4,18] and layered double hydroxides.[19]

In addition to the cost of the fabrication process, availability, biocompatibility, loading capacity, cytotoxicity, and controlled release rate are vital factors during the assessment of suitable drug carriers.[20] The natural species of zeolite minerals such as clinoptilolite are of massive natural reserves and low mining cost.[21,22] They possess remarkable biocompatibility, ion-exchange capacity, non-toxicity, chemical stability, surface area, and loading adsorption capacity.[23,24] Moreover, they possess anti-diarrheal, hemostatic, and anti-oxidative properties in addition to their support effect on immune activity.[25] Such technical, physicochemical, and biological properties qualify most of the natural zeolite species to be used as carriers for cancer chemotherapies, considering both the loading and the release properties.[26,27] However, it was reported that the surface functionalization, modification, and nanoparticle decoration of the microporous structures of natural zeolite minerals cause significant enhancement for their technical specifications either as drug carriers or as adsorbents.[28]

Calcium oxide (CaO) nanoparticles are one of the reliable metal oxide nanoparticles widely used in several biomedical and environmental applications.[11,29,30] This is related to their eco-friendly properties, high chemical activity, low fabrication cost, low solubility, low toxicity, and high availability of their precursors.[31,32,8] The CaO particles can be produced by different physical, biological, thermal, and chemical techniques with different physicochemical properties.[8] The green and environmental synthesis methods were assessed and recommended widely in the later periods as simple, effective, and eco-friendly techniques.[34] The green synthesis processes involved using the extracts of plants, green leaves, vegetables, and algae as chemical reducing and oxidizing agents at room temperature.[34] The green synthesized particles by such techniques are safe materials with significant biodegradability, non-toxicity, reactivity, surface area, and low agglomeration properties.[33]

The green integration between clinoptilolite as a natural zeolite and CaO nanoparticles in the nanocomposite ($CaO_{(NP)}$/Clino) is an effective and biocompatible potential carrier for 5-FL drug with enhanced loading and release behaviors. Therefore, this study introduces new insight into the qualification of the green $CaO_{(NP)}$/Clino nanocomposite as a delivery system for the 5-FL drug. The study involved detailed investigation for the loading and release properties of the $CaO_{(NP)}$/Clino carrier as well as the affected mechanisms. Additionally, the cytotoxicity properties of $CaO_{(NP)}$/Clino and 5-FL-loaded $CaO_{(NP)}$/Clino were inspected for normal colorectal cells and cancer cells.

2. RESULTS AND DISCUSSION

2.1. Characterization of the $CaO_{(NP)}$/Clino Carrier. The starting zeolite shows the X-ray diffraction (XRD) pattern of clinoptilolite as a single phase with numerous diffraction peaks at 9.88, 11.18, 13, 14.91, 17.36, 19.02, 22.36, 22.7, 25, 26, 26.87, 28.15, 30, 32, 32.9, and 34° (JCPDS-card no., 98-000-2606) (Figure 1A). The pattern of $CaO_{(NP)}$/Clino composite demonstrates a remarkable declination in the number of zeolite diffraction peaks, and the residual peaks were identified as educed and fluctuated peaks at about 22.71, 28.15, and 30 (Figure 1B). Moreover, the loaded green CaO nanoparticles were identified by their characteristic peak at about 32.2° (JCPDS-card no., 00-004-0777) (Figure 1B). The

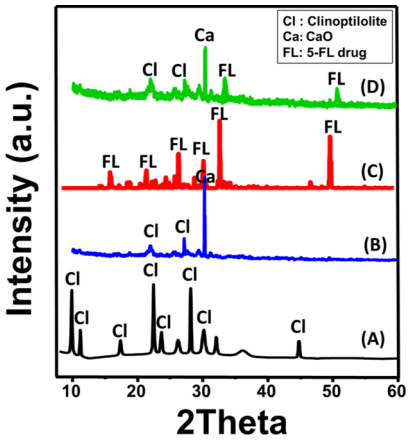

Figure 1. XRD patterns of raw clinoptilolite (A), synthetic $CaO_{(NP)}$/Clino nanocomposite (B), free 5-FL drug (C), and 5-FL-loaded $CaO_{(NP)}$/Clino (D).

pattern of 5-FL-loaded $CaO_{(NP)}$/Clino (Figure 1D) in comparison with the pure patterns of the 5-FL drug (Figure 1C) and the $CaO_{(NP)}$/Clino composite declared the successful loading of the drug. The crystalline peaks of the 5-FL drug were observed as much reduced diffraction peaks (Figure 1D). This suggested the role of the $CaO_{(NP)}$/Clino composite as a carrier in promoting the amorphization properties of the 5-FL drug as well as its solubility.

Considering the scanning electron microscopy (SEM) images of both clinoptilolite and the $CaO_{(NP)}$/Clino composite, there are remarkable changes in the morphological features. The clinoptilolite raw particles are clusters of aggregated flakey grains of smooth surfaces (Figure 2A,B). The $CaO_{(NP)}$/Clino particles are of new morphologies related to the loaded CaO nanoparticles. The surface of the zeolite substrate was covered by highly oriented CaO nanorods that were detected parallel and attached to each other (Figure 2C,D). This is of positive effect on both the dispersion properties and the surface area of $CaO_{(NP)}$/Clino as a carrier for the 5-FL drug. The surface area enhanced from 252.4 m^2/g for Clino particles to 258 m^2/g for the synthetic $CaO_{(NP)}$/Clino particles. The measured particle size of Clino particles ranged from 4 to 6 μm, while the particle size of $CaO_{(NP)}$/Clino ranged from 0.6 μn to 300 nm. The declination in the particle size distribution reflected the influence of the sonication waves during the synthesis processes on dispersing the agglomerated particles from each other. Additionally, the average pore diameter of clinoptilolite was reduced from about 18.2 nm to about 15.4 nm after loading its structure with green CaO. This reflected partial blocking for the pores of zeolite by the CaO nanoparticles.

The FT-IR spectra of Clino particles, $CaO_{(NP)}$/Clino, and 5-FL-loaded $CaO_{(NP)}$/Clino demonstrate clearly the chemical interaction during the synthesis and loading processes. The essential chemical groups of clinoptilolite (OH (3442 cm^{-1}), zeolite-trapped water (1640 cm^{-1}), T−O bonds of structural TO_4 tetrahedrons (1041 cm^{-1}), and the O−T−O or T−O group (T = Al and/or Si) (467 cm^{-1})) were detected clearly from its FT-IR spectrum (Figure 3A).[34,35] After the synthesis of $CaO_{(NP)}$/Clino, the obtained spectrum declared the presence of the same chemical groups but with deviated bands and remarkable intensification for the OH-related bands (Figure 3B). The intensification in the OH-bearing groups is related to the influence of the alkaline conditions on inducing

https://doi.org/10.1021/acsomega.1c04725
ACS Omega 2021, 6, 31982−31992

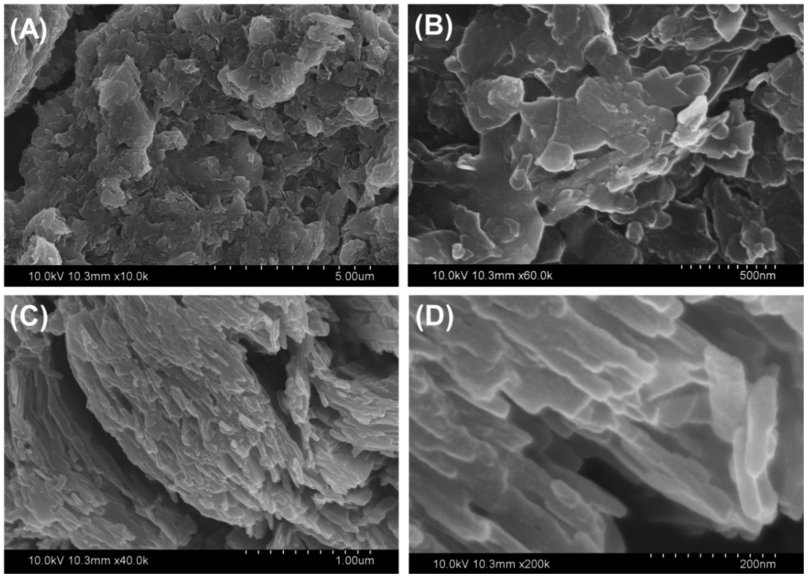

Figure 2. SEM images of raw clinoptilolite (A,B) and SEM images of $CaO_{(NP)}$/Clino green nanocomposite (C,D).

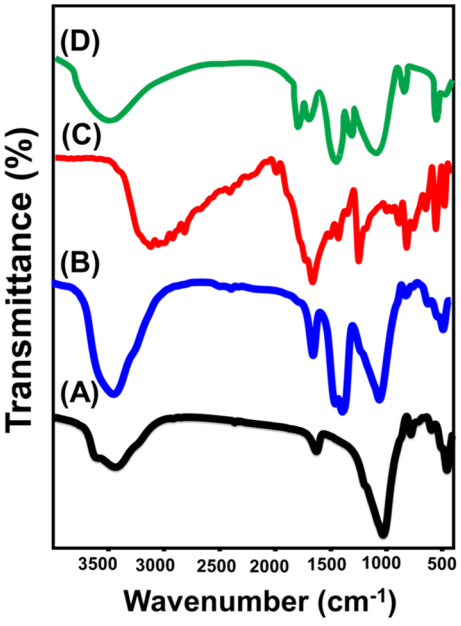

Figure 3. FT-IR spectra of raw clinoptilolite (A), synthetic $CaO_{(NP)}$/Clino nanocomposite (B), free 5-FL drug (C), and 5-FL-loaded $CaO_{(NP)}$/Clino (D).

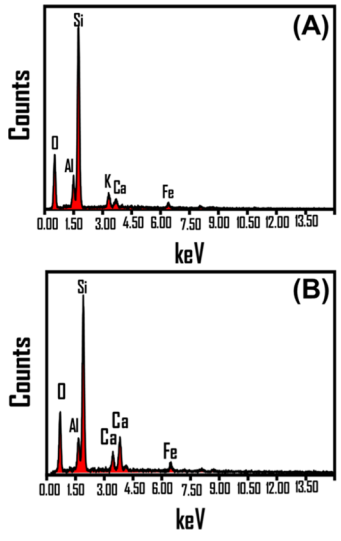

Element	Mass%	Atom%
O	46.64	62.19
Al	7.21	5.70
Si	36.28	27.56
K	3.43	1.87
Ca	1.98	1.05
Fe	3.01	1.15

Element	Mass%	Atom%
O	50.77	66.71
Al	5.85	4.56
Si	28.94	21.66
K	3.46	1.86
Ca	7.31	3.83
Fe	3.68	1.38

Figure 4. EDX spectra and elemental composition of raw clinoptilolite (A) and synthetic $CaO_{(NP)}$/Clino (B).

the exposure of the silanol groups such as Al−OH and Si−OH (Figure 3B).[36] Additionally, two new bands were identified at 742 and 517 cm^{-1} related to the CaO and C−O groups of the loaded green calcium oxide (Figure 3B).[31] The spectrum of 5-FL-loaded $CaO_{(NP)}$/Clino (Figure 3D) in comparison with the spectra of the free 5-FL drug (Figure 3C) and $CaO_{(NP)}$/Clino declared the successful loading of the drug. The spectrum of the 5-FL-loaded $CaO_{(NP)}$/Clino composite demonstrates the existence of N−H (542 cm^{-1}), CF═CH (782.4 cm^{-1}), and C═O (1784.5 cm^{-1}) groups that related to the 5-FL drug in addition to the essential groups of clinoptilolite but at shifted positions (Figure 3D).[1]

The elemental composition of both Clino particles and the $CaO_{(NP)}$/Clino composite was studied based on their EDX spectra (Figure 4). The clinoptilolite sample is composed of Si (36.28%), Al (7.21%), O (46.64%), K (3.43%), Ca (1.98%), and Fe (3.01%) (Figure 4A). Based on the EDX spectrum of $CaO_{(NP)}$/Clino composite, the calcium content increased to 7.3% and the oxygen content increased to 50.77%, which is related to the loaded CaO particles (Figure 4B). Partial leaching or substitution of both Al and Si ions by the Ca ions of the alkaline solution was suggested based on the decrease in their contents to 5.85 and 28.49%, respectively (Figure 4B). This affected the ion-exchange properties as the capacity increased from 132 meq/100 g for Clino particles to 134.4 meq/100 g for the synthetic $CaO_{(NP)}$/Clino green composite. The enhancement in the ion-exchange capacity will be of vital impact in enhancing the loading and release behaviors of $CaO_{(NP)}$/Clino as a carrier for the 5-FL drug.

2.2. Loading Properties of $CaO_{(NP)}$/Clino for the 5-FL Drug. *2.2.1. Effect of Loading Factors. 2.2.1.1. Effect of Loading pH.* The pH of the loading reaction shows direct and strong effect on the loading properties of both Clino and $CaO_{(NP)}$/Clino composites. This is credited mainly to the

https://doi.org/10.1021/acsomega.1c04725
ACS Omega 2021, 6, 31982−31992

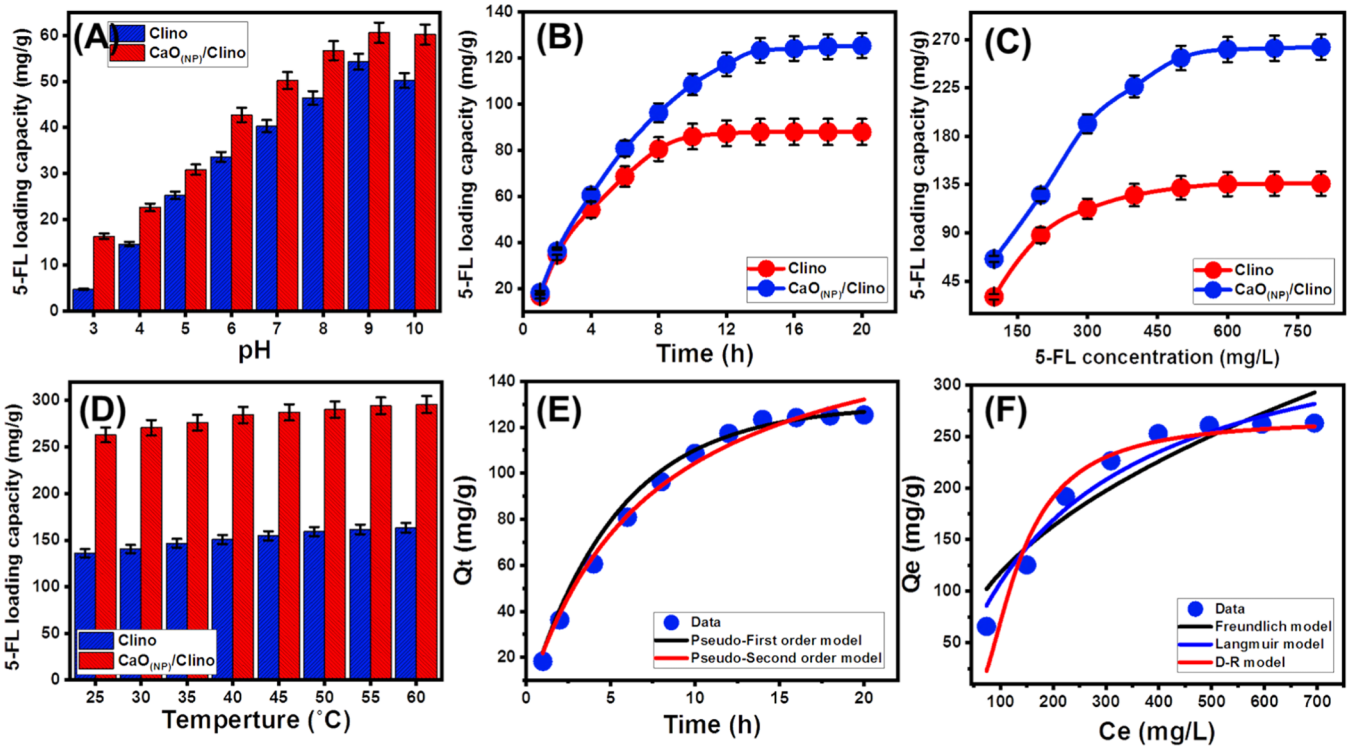

Figure 5. Influence of pH on the loading capacity of 5-FL (A), effect of loading interval on the loading capacities of 5-FL (B), effect of 5-FL concentrations on the achieved loading capacity (C), effect of temperature on the loading capacity of 5-FL (D), fitting of the loading results with the kinetic models (E), and fitting of the 5-FL loading results with the isotherm models (F).

controlled impact of pH value on the speciation behavior of the drug as dissolved ions and the dominant charges on the surface of $CaO_{(NP)}$/Clino as the solid carrier. The pH as a factor was followed from pH 3 until pH 10, and the main factors were fixed at 4 h, 200 mg/L, 25 °C, and 20 mg for the 5-FL loading time, 5-FL concentration, the temperature of the test, and the dosage of the carriers (Figure 5A). The measured 5-FL loading capacities of Clino and $CaO_{(NP)}$/Clino enhanced strongly by increasing the pH of the tests from pH 3 until pH 9 (Figure 5A). Therefore, the best 5-FL loading pH is pH 9 (alkaline environment), and the measured capacities at this value are 54.3 and 60.6 mg/g for Clino and $CaO_{(NP)}$/Clino, respectively (Figure 5A). The alkaline conditions induce the ionization of 5-FL drug into structures of more stable properties and cause an increase in ionic interactions as a result of the complete ionization of the 5-FL molecules.[37,38] Beyond pH 9, both Clino and $CaO_{(NP)}$/Clino shows observable declination in their 5-FL loading capacities. This might be assigned to the oversaturation of their surfaces with negative hydroxyl radicals or the partial destruction of the carriers as silicate structures at such high alkaline conditions.[18,39] The previous findings were supported by the determined $pH_{(PZC)}$ value of $CaO_{(NP)}$/Clino as it is equal to 6.2, which signify the saturation of the composite surface by negative charges above this pH value (pH 6.2).

2.2.1.2. Effect of the Loading Interval. The effect of 5-FL loading intervals on the loading behaviors of Clino and $CaO_{(NP)}$/Clino was inspected from 1 h until 20 h, and the main factors were fixed at pH 9, 200 mg/L, 25 °C, and 20 mg for the pH environment, 5-FL concentration, the temperature of the test, and the dosage of the carriers, respectively. There is an observable enhancement in the measured capacities with increasing 5-FL loading time for Clino and $CaO_{(NP)}$/Clino until 10 h and 14 h, respectively (Figure 5B). After these intervals, the measured 5-FL loading capacities appear to be fixed values or of slight changes, which can be classified as the equilibrium stages (Figure 5B). The recognized 5-FL equilibrium loading capacities of Clino and $CaO_{(NP)}$/Clino are 88 mg/g and 125.4 mg/g, respectively (Figure 5B). This behavior as a function of the 5-FL loading time was assigned to the presence of numerous free active loading receptors during the initial 5-FL loading intervals, which resulted in high loading rates.[1,20] With expanding the 5-FL loading time, the available free receptors were consumed regularly by the adsorbed 5-FL molecules, and the loading process became restricted to the remaining receptors.[11] Therefore, the 5-FL loading rate declined significantly, and the complete occupation of all the receptors resulted in the equilibration stage that exhibits nearly fixed loading rates and capacities.

2.2.1.3. Effect of 5-FL Concentration. The 5-FL concentration as an experimental loading factor was assessed to follow the equilibrium properties of the reactions as well as the loading capacities of Clino and $CaO_{(NP)}$/Clino carriers. The effect of 5-FL concentration was inspected from 100 mg/L until 800 mg/L, and the main factors were fixed at pH 9, 20 h, 25 °C, and 20 mg for the pH environment, 5-FL loading time, the temperature of the test, and the dosage of the carriers, respectively (Figure 5C). The measured 5-FL loading properties of Clino and $CaO_{(NP)}$/Clino were induced significantly by inspecting their capacities at high concentrations of 5-FL (Figure 5C). This behavior was reported in the literature as a result of the acceleration in the mass-transfer rates and driving forces of the 5-FL molecules by conducting the tests at high concentrations of the drug.[33,37] Such enhancement in the 5-FL capacities was detected until the inspected concentration of 600 mg/L is the same as the

https://doi.org/10.1021/acsomega.1c04725
ACS Omega 2021, 6, 31982−31992

experimental equilibrium concentration (Figure 5C). At such concentration, the Clino and $CaO_{(NP)}$/Clino carriers achieve their maximum capacities (136 mg/g (Clino) and 263 mg/g ($CaO_{(NP)}$/Clino) as all the present receptors were consumed by the adsorbed 5-FL molecules (Figure 5C).

2.2.1.4. Effect of Loading Temperature. The temperature effect on the 5-FL loading properties of Clino and $CaO_{(NP)}$/Clino was assessed from 25 °C until 60 °C, and the main factors were fixed at pH 9, 20 h, 800 mg/L, and 20 mg for the pH environment, 5-FL loading time, 5-FL concentration, and the dosage of the carriers (Figure 5D). There is an obvious increment in the measured 5-FL loading capacities of Clino and $CaO_{(NP)}$/Clino carriers by increasing the test temperature up to 60 °C (Figure 5D). The determined 5-FL loading capacities at this temperature are 163.3 and 295.8 mg/g for Clino and $CaO_{(NP)}$/Clino, respectively (Figure 5D). Therefore, the loading processes of 5-FL into Clino and $CaO_{(NP)}$/Clino as carriers are of endothermic properties.

Considering the presented loading results, the $CaO_{(NP)}$/Clino green nanocomposite as a carrier is of enhanced loading capacity than clinoptilolite as a single phase. Such observable enhancement is related mainly to the remarkable increase in the composite surface area and ion-exchange capacity. Additionally, the existence of complex active functional groups that are related to both the clinoptilolite substrate and the loaded CaO is of strong impact in inducing the loading capacity of the $CaO_{(NP)}$/Clino green nanocomposite.

2.2.2. Loading Mechanism. 2.2.2.1. Kinetic Studies. The kinetic properties of the 5-FL loading reactions using CaO (NP)/Clino as a carrier were addressed, considering the assumption of both pseudo-first-order (P.F.) and pseudo-second-order (P.S.) kinetic models (Figure 5E and Table 1). The non-linear fitting processes with the models declared a slightly higher fitting degree with the P.F. model than the P.S. model, considering the recognized values of both correlation coefficients (R^2) and Chi-squared (χ^2) (Figure 5E and Table 1). Therefore, the loading of 5-FL into $CaO_{(NP)}$/Clino follows the kinetic hypothesis of both models, and occurred reactions involved complex physical (electrostatic attractions) and chemical (chemical complex, ion exchange, hydrogen bonding, and internal diffusion) mechanisms.[20,40]

2.2.2.2. Equilibrium Studies. Freundlich and Langmuir isotherm models in addition to the Dubinin−Radushkevich model (D−R) were inspected to follow the equilibrium behavior of 5-FL loading reactions into the $CaO_{(NP)}$/Clino carrier (Figure 5F and Table 1). The non-linear fitting processes with the models emphasized a remarkable higher fitting degree with the Langmuir model than the Freundlich model, considering the recognized values of both correlation coefficient (R^2) and Chi-squared (χ^2) (Figure 5F and Table 1). Therefore, the occurred 5-FL loading reactions are of Langmuir equilibrium behavior. This involved loading of the 5-FL molecules in the monolayer formed by homogeneous active loading receptors on the surface of $CaO_{(NP)}$/Clino as a solid carrier.[4] Considering the values of RL as theoretical parameters for the Langmuir model, the loading reactions of 5-FL by $CaO_{(NP)}$/Clino are of favorable properties. Additionally, the theoretical maximum 5-FL loading capacity of the $CaO_{(NP)}$/Clino carrier is 305.2 mg/g, suggesting the possible enhancement for the loading capacity of the carrier by more adjusting the conditions, considering the experimentally obtained value 263 mg/g at the same conditions (25 °C) and 295.8 mg/g at 60 °C.

Table 1. Theoretical Parameters of the Studied Kinetic Models, the Equilibrium Models, the Van't Hoff Formula, and the Release Kinetic Models

model	parameters	
pseudo-first-order	K_1 (min^{-1})	0.1888
	$q_{e\ (Cal)}$ (mg/g)	129.7
	R^2	0.99
	X^2	0.7
pseudo-second-order	k_2 (g mg^{-1} min^{-1})	7.68×10^{-4}
	q_e (Cal) (mg/g)	142.6
	R^2	0.98
	X^2	1.73
Isotherm models		
Langmuir	q_{max} (mg/g)	305.2
	b (L/mg)	0.0039
	R^2	0.94
	X^2	3.21
	R_L	0.24−0.71
Freundlich	$1/n$	0.469
	k_F (mg/g)	13.57
	R^2	0.86
	X^2	4.12
D−R model	β (mol^2/KJ^2)	0.0059
	q_m (mg/g)	267
	R^2	0.91
	X^2	3.65
	E (KJ/mol)	9.2
Thermodynamics		
$\Delta G°$ (kJ mol^{-1})	298.15	−14.7
	303.15	−15.04
	308.15	−15.35
	313.15	−15.69
	318.15	−15.97
	323.15	−16.25
	328.15	−16.55
	333.15	−16.82
$\Delta H°$ (kJ mol^{-1})		2.96
$\Delta S°$ (J K^{-1} mol^{-1})		60.2

release kinetics	determination coefficient	
models	pH 1.2	pH 7.4
zero-order model	0.85	0.77
first order model	0.98	0.96
Higuchi model	0.90	0.92
Hixson−Crowell model	0.96	0.94
Korsmeyer−Peppas model	0.95	0.95

The fitting process with the D-R model and the related parameters were used to signify the nature of the occurred 5-FL loading reactions (Figure 5F and Table 1). The estimated Gaussian energy for the 5-FL loading reaction into the $CaO_{(NP)}$/Clino carrier is 9.2 KJ/mol, and this value is related to chemical loading reactions but still close to the upper limit of the physical loading processes (Table 1).[28] This is of considerable agreement with the kinetic findings; additionally, the values are within the suggested levels for the Gaussian energy of the ion-exchange processes within the zeolite structures.[33]

2.2.2.3. Thermodynamic Studies. The thermodynamic parameters including Gibbs free energy ($\Delta G°$), enthalpy ($\Delta H°$), and entropies ($\Delta S°$) were used to describe the thermodynamic properties of $CaO_{(NP)}$/Clino as a carrier for

https://doi.org/10.1021/acsomega.1c04725
ACS Omega 2021, 6, 31982−31992

the 5-FL drug. The ΔG° parameter is calculated directly from eq 1, while the ΔH° and ΔS° parameters were obtained theoretically from the fitting process with the Van't Hoff equation (eq 2) (Figure 6).

$$\Delta G^\circ = -RT \ln K_c \quad (1)$$

$$\ln(K_c) = \frac{\Delta S^\circ}{R} - \frac{\Delta H^\circ}{RT} \quad (2)$$

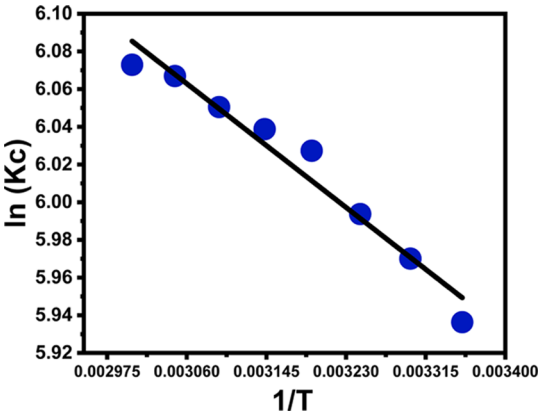

Figure 6. Fitting of the 5-FL loading results by $CaO_{(NP)}$/Clino with the Van't Hoff equation.

The negatively signed values of ΔG° emphasize the nature of the 5-FL loading process by spontaneous, feasible, and favorable loading reactions[41] (Table 1). The positively signed value of the ΔH° parameter reflects the endothermic properties of the occurred 5-FL loading reaction (Table 1). Moreover, the positively signed value of the entropy (ΔS°) parameter suggested the increment in the randomness behavior of the 5-FL loading reaction by performing the tests at high temperature (Table 1).

2.3. Release Properties of CaO $_{(NP)}$/Clino. *2.3.1. Release Profile of the 5-FL Drug.* The 5-FL release profiles of $CaO_{(NP)}$/Clino in comparison with pure Clino particles as carriers were assessed, considering two releasing buffers [intestinal fluid (pH 7.4) and gastric fluid (pH 1.2)] (Figure 7). The release curves of both Clino and $CaO_{(NP)}$/Clino show remarkably two segments declaring differences in the release rates with time (Figure 7). The first release segment either at the gastric or the intestinal fluids declared a fast release rate for 5-FL from both Clino and $CaO_{(NP)}$/Clino. This release behavior is attributed to the diffused 5-FL molecules from the surficial loading receptors of both Clino and $CaO_{(NP)}$/Clino.[10] The second stages or segments show slow 5-FL release rates and cover the later intervals of the release profiles (Figure 7). The detection of this segment reflected slow diffusion for the entrapped 5-FL molecules within the structural channels of zeolite.[42,43]

For the Clino particles, it exhibits slow and long release profiles for about 150 h either at pH 7.4 or at pH 1.2 without complete diffusion for the loaded 5-FL dosage (Figure 7A,B). The determined maximum 5-FL release percentages were detected after 70 h and 100 h at pH 1.2 (66.4%) and pH 7.4 (73%), respectively. The observed very slow release rate for the 5-FL drug from the structure of Clino particles in the inspecting release buffers was assigned to (a) the deep entrapment of 5-FL molecules within the structural nanopores

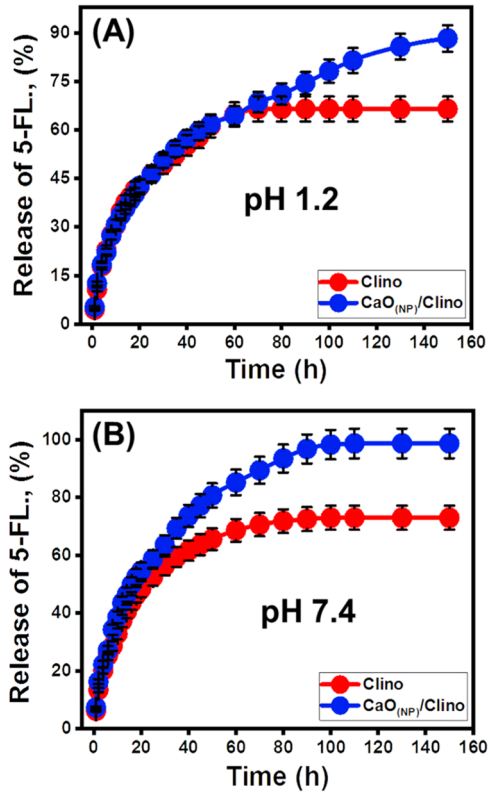

Figure 7. Release profiles of Clino and $CaO_{(NP)}$/Clino nanocomposite as carriers for 5-FL at pH 1.2 (A) and pH 7.4 (B).

of clinoptilolite and (b) the predicted formation of hydrogen bonds between the active chemical groups of the 5-FL drug and the active siloxane groups of clinoptilolite.[28,44] The higher diffusion of the 5-FL drug at pH 7.4 than at pH 1.2 was explained to be related to the ionization behavior of the drug at such pH values, which induce its diffusion and solubility properties.[44,6] Such very slow profiles suffer from remarkable drawbacks as the loaded 5-FL dosage will not diffuse at the required level, which will increase the amount or the number of dosages.

The recognized 5-FL release profiles of $CaO_{(NP)}$/Clino exhibit faster rates than the observed rates for Clino particles in its pure phases, considering the two releasing buffers [intestinal fluid (pH 7.4) and gastric fluid (pH 1.2)] (Figure 7A,B). Fifty percent of the loaded 5-FL dosage was diffused after 16 h and 30 h at pH 7.4 and pH 1.2, respectively. About 95% of the loaded 5-FL dosage was diffused after 90 h at pH 7.4 (intestinal fluid), while the maximum release 5-FL percentage (88%) was obtained after 180 h. Such profiles considering the two diffusion buffers qualify the studied $CaO_{(NP)}$/Clino green nanocomposite to be used as potential delivery for the 5-FL drug at a controlled rate, specific intervals, and adjusted therapeutic dosage. The faster 5-FL diffusion rates of $CaO_{(NP)}$/Clino as compared to the observed rates for Clino particles declare the effect of the loaded CaO green nanorods on acting as partial blocking surface for the structural nanopores of zeolite. This hinders effectively the entrapment probabilities of the loaded 5-FL drug within the pores in addition to the role of CaO cover on declining the numbers of the formed bonds (hydrogen bonds) between the chemical structure of the drug and the structural siloxane groups of zeolite (clinoptilolite substrate).

https://doi.org/10.1021/acsomega.1c04725
ACS Omega 2021, 6, 31982−31992

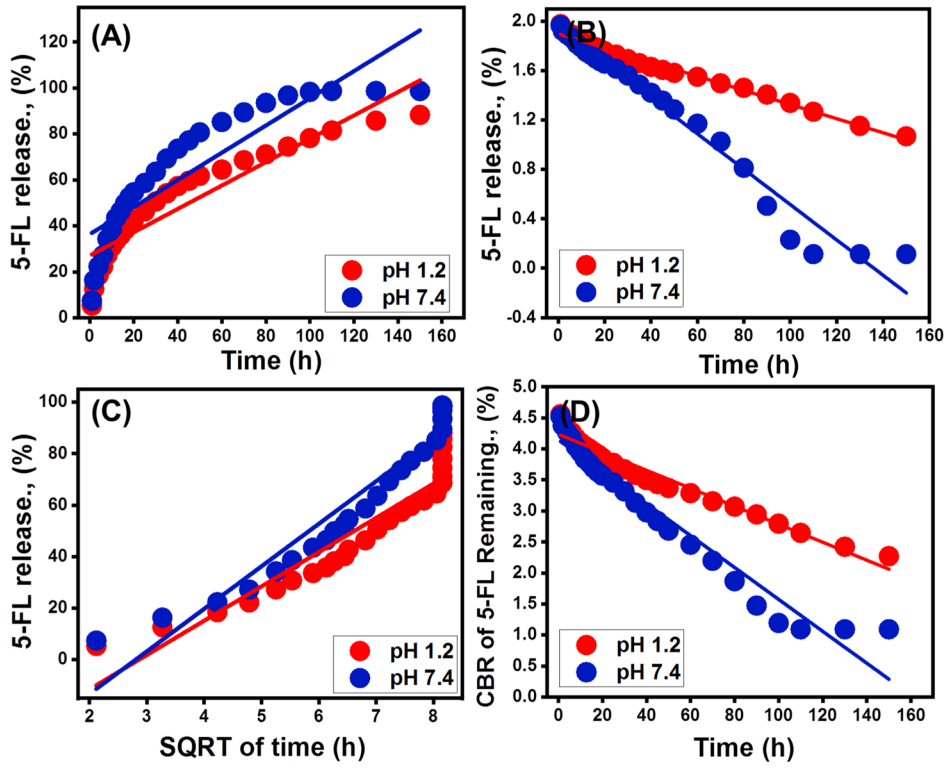

Figure 8. Fitting of the 5-FL release results from nanocomposites with zero-order model (A), first-order model (B), Higuchi model (C), and Hixson−Crowell model (D).

2.3.2. Release Kinetics. The kinetic properties of the occurred 5-FL release reactions from $CaO_{(NP)}$/Clino as a carrier were assessed, considering the assumptions zero-order (eq 3), first-order (eq 4), Higuchi (eq 5), Hixson−Crowell (eq 6), and Korsmeyer−Peppas (eq 7).[20]

$$W_t - W_0 = K_0 \cdot t \tag{3}$$

$$\ln(W_\infty / W_t) = K_1 \cdot t \tag{4}$$

$$W_t = K_h t^{1/2} \tag{5}$$

$$W_o^{1/3} - W_t^{1/3} = K_{HC} t \tag{6}$$

$$W_t / W_\infty = K_p t^n \tag{7}$$

The release reactions with zero-order properties exhibit a constant diffusion rate without a significant impact on the drug dosages. However, the release systems with first-order properties are controlled strongly by the dosages of the loaded drug.[1,45] For the release properties of Higuchi kinetics, the release of the 5-FL drug occurred by diffusion processes according to six basics. The release basics of this model are as follows: (A) the loaded 5-FL dosage is higher than the measured diffusion rate, (B) there is one direction controlled the diffusion process, (C) the diameter of 5-FL as the loaded drug is smaller than the thickness of $CaO_{(NP)}$/Clino as a carrier, (D) the swelling, as well as the solubility of the used carrier, has impact on the diffusion rates, (E) the diffused 5-FL drug exhibits a constant rate, and (F) the assessed 5-FL molecules possess sink properties.[1,28] The release system with the Hixson−Crowell kinetics exhibits the release properties of the erosion mechanism. Additionally, the release efficiency depends essentially on both the diatomite of the $CaO_{(NP)}$/Clino particles and the surface area.[42] The release systems with Korsmeyer−Peppas kinetics are controlled by both diffusion and erosion mechanisms.[28]

The results of the fitting processes declared higher agreement between the 5-FL release process from $CaO_{(NP)}$/Clino with the first-order model (Figure 8B and Table 1) than the zero-order model (Figure 7A and Table 1). This declared a significant effect for the 5-FL concentration on the release efficiency from the $CaO_{(NP)}$/Clino carrier either at pH 1.2 (Gastric fluid) and at pH 7.4 (Intestinal fluid). Considering the high fitting degrees with both Higuchi (Figure 7C) and Hixson−Crowell kinetic models (Figure 8D and Table 1), the release of 5-FL drug from the $CaO_{(NP)}$/Clino carrier involves the complex processes of erosion and diffusion mechanisms. The erosion mechanism might be related to the partial dissolving of CaO at the acidic fluid [gastric (pH 1.2)] and the partial leaching of the zeolitic structural elements at the basic fluid [intestinal fluid (pH 7.4)]. This suggestion was supported by the high fitting degrees with the Korsmeyer−Peppas model (Figure S1 and Table 1). The estimated diffusion exponent (n) as a parameter of the model (0.49 at pH 1.2 and 0.48 at pH 7.4) suggested the release of 5-FL drug according to the non-Fickian transport, suggesting complex erosion and diffusion mechanisms.[11]

2.4. Comparison Study. The 5-FL loading and release properties of $CaO_{(NP)}$/Clino were compared with the other findings in the literature and clinoptilolite as the pure phase (Table 2). The synthetic $CaO_{(NP)}$/Clino carrier achieved higher 5-FL loading capacities than most of the investigated carriers in the literature with a q_{max} of 305.2 mg/g (Table 2). Such properties have essential commercial and technical impact to control the dosages of the loaded 5-FL and to reduce the required quantities of the addressed carrier. Additionally, this has a direct effect on reducing the

https://doi.org/10.1021/acsomega.1c04725
ACS Omega 2021, 6, 31982−31992

Table 2. Comparison between the Loading Capacities and Release Periods of the Studied Carrier and Other Carriers in the Literature

carrier	loading capacity (mg/g)	release period	refs
montmorillonite/magnetite	59.44	24 h	18
Ca-montmorillonite	23.3		46
HY zeolite	110	5 h	47
magadiite	98.18		48
montmorillonite	90		49
magadiite-CTAB-chitosan	162.29		48
magadiite-CTAB	130.59		48
chitosan/MCM-48	191	80 h	11
kaolinite nanotubes	103	60 h	3
clinoptilolite	138.9	150 h	this study
$CaO_{(NP)}$/Clino	305.2	150	this study

concentrations of the discharged 5-FL drug as pharmaceutical residuals during the loading processes. $CaO_{(NP)}$/Clino exhibits long and continuous release properties (150 h) as compared to the other studied carriers (Table 2). This reflects the values of the composite to introduce 5-FL as a loaded drug at a fixed rate and at a specific dosage according to the therapeutic requirements. Moreover, the 5-FL release rate can be controlled based on the ratio of the integrated green CaO in the composite.

2.5. Cytotoxicity Results. The cell viability properties of $CaO_{(NP)}$/Clino and 5-FL-loaded $CaO_{(NP)}$/Clino were evaluated by the MTT assay method, considering both the normal cells [colorectal fibroblast (CCD-18Co)] and the cancer cells [colon cancer cells (HCT-116)] (Figure 9). The free $CaO_{(NP)}$/Clino green nanocomposite possess high safety properties and acceptable cytotoxic effect on the normal colorectal cells. The measured cell viability values are not lower than 86.5% in the presence of the maximum dosage (300 μg/mL), reflecting the significant biocompatible properties of the synthetic $CaO_{(NP)}$/Clino (Figure 9A).

The measured cell viability values of the tested cancer cells (HCT-116) in the presence of the free 5-FL drug, free $CaO_{(NP)}$/Clino, and the 5-FL-loaded $CaO_{(NP)}$/Clino were plotted graphically in Figure 9B. Based on the plotted data, the measured cell viability shows observable declination in the values with the regular incorporation of the drug and the materials as higher dosages up to 300 μg/mL (Figure 9B). The cell viability of HCT-116 using 5-FL-loaded $CaO_{(NP)}$/Clino is lower than that of the free 5-FL drug at all the assessed dosages (Figure 9B). The measured cell viability values at the highest dosages (300 μg/mL) of free 5-FL drug and 5-FL-loaded $CaO_{(NP)}$/Clino are 34 and 12.4%, respectively (Figure 9B). This declares observable enhancement for the cytotoxic effect of the drug after loading it into $CaO_{(NP)}$/Clino as a carrier. Such enhancement can be assigned to (A) the distribution of the loaded 5-FL molecules in a homogeneous form on the structure of zeolite and CaO nanorods induce the interaction surface area, (B) the regular diffusion rate of the 5-FL molecules enhances their effects on the studied cells, and (C) the oxidation properties of CaO show considerable oxidative stress on HCT-116 cells. The measured cell viability values using free $CaO_{(NP)}$/Clino support the suggested role of the composite as a carrier and the oxidation effect of CaO (Figure 9B). Therefore, the application of the $CaO_{(NP)}$/Clino green nanocomposite as a carrier for 5-FL has valuable effect on inducing the solubility, biocompatibility, safety, and cytotoxicity properties as chemotherapy for colon cancer.

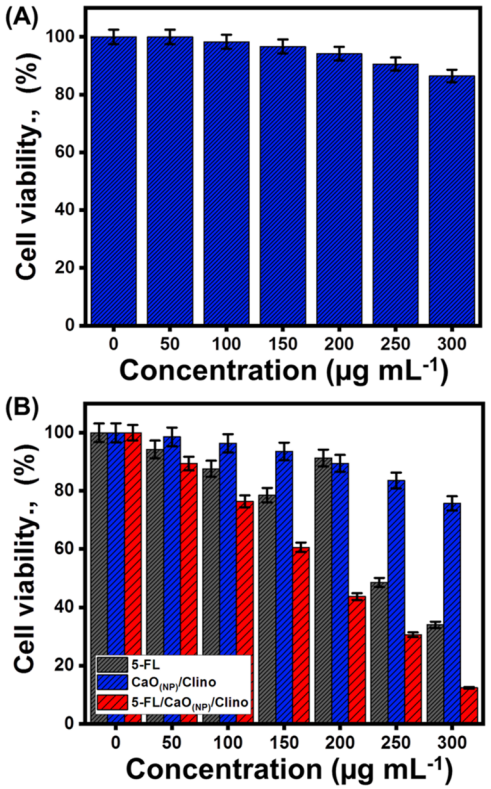

Figure 9. In vitro cytotoxicity effect of $CaO_{(NP)}$/Clino carrier on the normal colorectal fibroblast cell (CCD-18Co) (A) and cytotoxicity effect of free 5-FL drug, free $CaO_{(NP)}$/Clino, and 5-FL-loaded $CaO_{(NP)}$/Clino on colon cancer cells (HCT-116) (B).

3. CONCLUSIONS

Sonocogreen CaO/clinoptilolite nanocomposite ($CaO_{(NP)}$/Clino) was assessed as an enhanced carrier for the 5-FL drug, considering the loading and release properties as well as the cytotoxic effect. The $CaO_{(NP)}$/Clino carrier has a loading capacity of 305.2 mg/g as that of 5-FL, which is an enhanced value considering the studied clinoptilolite and other carriers in the literature. The assumptions of pseudo-first-order and Langmuir models were used to illustrate the kinetic and equilibrium behavior of the 5-FL loading reactions. Considering the equilibrium and thermodynamic parameters, the 5-FL loading reactions possess homogeneous, spontaneous, monolayer, endothermic, and more chemical properties. The $CaO_{(NP)}$/Clino release profile extends regularly for 150 h either at pH 1.2 (gastric fluid) or at pH 7.4 (Intestinal fluid). The operated mechanisms during the release of the 5-FL drug involved complex erosion and diffusion processes and follow the kinetics of Higuchi, Hixson–Crowell, and Korsmeyer–Peppas models. The CaO(NP)/Clino carrier exhibits a promising biocompatible and safe value based on the measured cell viability results for colorectal normal cells (CCD-18Co). Additionally, it has direct impact in inducing the cytotoxic effect of the drug on colon cancer cells (HCT-116).

https://doi.org/10.1021/acsomega.1c04725
ACS Omega 2021, 6, 31982−31992

4. EXPERIMENTAL SECTION

4.1. Materials. Clinoptilolite zeolite with a chemical composition of SiO_2 (68.39 wt %), K_2O (4.06 wt %), Fe_2O_3 (2.67%), CaO (1.65 wt %), Al_2O_3 (11.5 wt %), MgO (0.48 wt %), Na_2O (0.38 wt %), and L.O.I (10.99 wt %) was obtained from the Al-Ahyuq zeolite mine, Taiz city, Yemen. Calcium nitrate tetrahydrate ($Ca(NO_3)_2.4H_2O$) of 97% purity was obtained from Sigma-Aldrich, Egypt. Commercial green tea leaves were used in the preparation of its green extract as a natural capping and reducing agent during the synthesis process for its content of polyphenols and caffeine. 5-FL drug ($C_4H_3FN_2O_2$) of 99% purity was delivered from Sigma-Aldrich Company (CAS number: 51-21-8; Pk_a: 8.02) which can be used during the release and loading experiments.

4.2. Synthesis of Green $CaO_{(NP)}$/Clinoptilolite Nanocomposite ($CaO_{(NP)}$/Clino). Clinoptilolite zeolite (Clino) was ground extensively for about 8 h. Then, the ground Clino (5 g) was homogenized with a pre-prepared aqueous solution (50 mL) of calcium nitrate tetrahydrate (2.5 g of Ca salt). The homogenization process involved stirring at 500 rpm and sonication irradiation at a power of 240 W at pH 8 for 90 min and at a certain temperature of 25 °C. At the same time, the extract solution of the green tea leaves was prepared by gentle boiling of the leaves for 5 min in distilled water. The extract (50 mL) was then mixed with the zeolite/Ca suspension (50 mL), considering the reaction conditions under stirring for 120 min and sonication treatment for another 120 min. The obtained mixture was aged for 24 h at room temperature to achieve the best interaction and loading of the CaO nanoparticles on the surface of clinoptilolite. As a final step, the solid particles of the green composite were separated from the reacting solutions, washed effectively, and dried in an electric oven at 70 °C for a certain interval of 12 h and used in further tests.

4.3. Characterization of the $CaO_{(NP)}$/Clino Carrier. The crystal structures and the change in the formed crystalline phases were studied, considering the XRD patterns of Clino, $CaO_{(NP)}$/Clino, and 5-FL-loaded $CaO_{(NP)}$/Clino, which were obtained using a PANalytical X-ray diffractometer (Empyrean) from 5 to 70° at an operation voltage of 40 kV. The changes in the surface features and the general morphology were studied using a scanning electron microscope (Gemini, Zeiss-Ultra 55). The elemental composition and the structural chemical groups were studied using an energy-dispersive X-ray spectrometer and a Fourier transform infrared spectrometer (FTIR−8400S), respectively, within the detection frequency range from 400 to 4000 cm^{-1} at a fixed scan of 37° and a resolution value of 4 cm^{-1}. The microstructural properties including the porosity and the surface area were measured by a surface area analyzer (Beckman Coulter; SA3100 type) after the degassing step at a measuring temperature of 77 K. A zetasizer device connected with a zeta cell (Malvern, version 7.11) was used as a system to measure the zeta potential of $CaO_{(NP)}$/Clino selected pH values, and then the results were used to detect the pH of zero point charge ($pH_{(ZPC)}$).

4.4. Loading Properties of $CaO_{(NP)}$/Clino. The loading properties of $CaO_{(NP)}$/Clino as a carrier for the 5-FL drug were assessed, considering the experimental ranges for the main factors [pH (pH 3 to pH 10), loading time (1−24 h), 5-FL concentration (100−900 mg/L), and temperature (25−60 °C)]. A vortex rotator was applied to mix the carrier particles with the 5-FL solutions. By the end of each loading experiment, the $CaO_{(NP)}$/Clino fractions were separated using a centrifuge and then filtrated to confirm the effective separation of the carrier particles. The residual 5-FL concentrations after the loading tests were detected after adjusting the wavelength at the λ (max) of the drug (266 nm). The tests were completed in triplicate form, and the plotted results are at their average values, considering the 5-FL loading capacities according to eq 8:

$$\text{loaded drug (mg/g)} = \frac{(\text{initial concentration} - \text{residual concentration}) \times \text{solvent volume}}{\text{carrier weight}} \quad (8)$$

4.5. In Vitro Release Profile. The release properties of $CaO_{(NP)}$/Clino as a carrier for 5-FL were followed using two types of buffers as release environments [gastric fluid (pH 1.2) in addition to intestinal fluid (pH 7.4)], considering the release temperature at 37.5 °C. A certain amount of 5-FL-loaded $CaO_{(NP)}$/Clino was mixed with the selected buffers (500 mL) for about 150 h as the total release period. The mixing and homogenization processes were performed using a dissolution apparatus (DISTEK type, 4300), and the container vessels were rotated at a fixed speed of 200 rpm. Then, 5 mL of each releasing buffer was isolated at different time intervals and analyzed to detect the concentrations of the loaded 5-FL molecules and were returned again to their bulk solutions. This was performed using a UV−vis spectrophotometer after adjusting the wavelength at the λ (max) of the drug (266 nm). The tests were completed in triplicate form, and the plotted results are at their average values, considering the 5-FL release percentages according to eq 9

$$\text{drug release (\%)} = \frac{\text{the amount of released 5-FL drug}}{\text{the amount of loaded 5-FL}} 100 \quad (9)$$

4.6. In Vitro Cytotoxicity Studies. *4.6.1. Cell Lines and Reagents.* Human colorectal fibroblast cells (CCD-18Co) and colon cancer cells (HCT-116) (ATCC, Rockville, MD) in addition to dimethyl sulfoxide (99%) (St. Louis, Mo., USA), *N*-(2-hydroxyethyl)piperazine-N′-ethanesulfonic acid buffer solution, 3(4,5-dimethylthiazol-2-yl)-2.5 diphenyltetrazolium bromide (MTT 99%) (St. Louis, Mo., USA), RPMI-1640, gentamycin, 0.25% Trypsin−ethylenediaminetetraacetate, fetal bovine serum, and Dulbecco's modified Eagle's medium were used during the cytotoxicity studies of the synthetic materials.

4.6.2. In Vitro Cytotoxicity. The cytotoxicity properties of $CaO_{(NP)}$/Clino as a carrier for 5-FL drug on both the normal and cancer colorectal cells were assessed as a vital factor to detect the influence of the carrier on inducing the safety and therapeutic effect of the loaded 5-FL drug. The assessed cell lines were first grown in a specific medium (RPMI-1640) supplemented with 50 μg/mL of gentamycin and 10% fetal calf serum, considering the growth environment of the humidified atmosphere (5% CO_2) and 37 °C. This system was sub-cultured three times per week, and then the cell lines were dispersed with Corning 96-well plates at a certain concentration of 5×10^4 cell/well and preserved under incubation for about 24 h. This was followed by the addition of both free $CaO_{(NP)}$/Clino particles and 5-FL-loaded particles with a studied concentration range from 0 μg/mL to 300 μg/mL. The systems were incubated for an additional 24 h, and the formed viable cells were measured by the MTT assay methods, considering the results of the control samples.

https://doi.org/10.1021/acsomega.1c04725
ACS Omega 2021, 6, 31982−31992

By the end of the adjusted exposure interval, the used culture medium was removed carefully to avoid its side effects and was replaced by a fresh culture medium (100 μL of RPMI). After that, 10 μL of MTT (12 mM) was added to the assessed cell wells and the control samples before the new incubation interval for about 5 h at the same growing environment. After a period, the formed formazan was dissolved carefully utilizing 50 μL of dimethyl sulfoxide. Finally, the optical densities of the samples were determined using a microplate reader after adjusting the wavelength at 590 nm. The obtained values were applied directly in the calculation of cell viability percentages based on eq 10.

$$\text{cell viability (\%)} = \frac{\text{mean OD}}{\text{control OD}} 100 \quad (10)$$

■ ASSOCIATED CONTENT

Supporting Information

The Supporting Information is available free of charge at https://pubs.acs.org/doi/10.1021/acsomega.1c04725.

Representative equation of the kinetic and isotherm models and fitting of the 5-FL release results with the Korsmeyer−Peppas model (PDF)

■ AUTHOR INFORMATION

Corresponding Author

Mostafa R. Abukhadra − *Geology Department, Faculty of Science and Materials Technologies and Their Applications Lab, Geology Department, Faculty of Science, Beni-Suef University, Beni-Suef City 62511, Egypt*; orcid.org/0000-0001-5404-7996; Email: Abukhadra89@Science.bsu.edu.eg

Authors

Alyaa Adlii − *Geology Department, Faculty of Science and Materials Technologies and Their Applications Lab, Geology Department, Faculty of Science, Beni-Suef University, Beni-Suef City 62511, Egypt*

Jong Seong Khim − *School of Earth & Environmental Sciences, College of Natural Sciences, Seoul National University, Seoul 08826, Republic of Korea*

Jamaan S. Ajarem − *Zoology Department, College of Science, King Saud University, Riyadh 11451, Saudi Arabia*

Ahmed A. Allam − *Zoology Department, Faculty of Science, Beni-Suef University, Beni-Suef 62511, Egypt*

Complete contact information is available at: https://pubs.acs.org/10.1021/acsomega.1c04725

Author Contributions

This article was written through the contributions of all authors. All authors have given approval to the final version of the manuscript.

Notes

The authors declare no competing financial interest.

■ ACKNOWLEDGMENTS

The authors acknowledge the Researchers Supporting Project number (RSP-2021/149), King Saud University, Riyadh, Saudi Arabia.

■ REFERENCES

(1) El-Zeiny, H. M.; Abukhadra, M. R.; Sayed, O. M.; Osman, A. H. M.; Ahmed, S. A. Insight into novel β-cyclodextrin-grafted-poly (N-vinylcaprolactam) nanogel structures as advanced carriers for 5-fluorouracil: Equilibrium behavior and pharmacokinetic modeling. *Colloids Surf., A* **2020**, *586*, 124197.

(2) Asgari, M.; Soleymani, M.; Miri, T.; Barati, A. A robust method for fabrication of monodisperse magnetic mesoporous silica nanoparticles with core-shell structure as anticancer drug carriers. *J. Mol. Liq.* **2019**, *292*, 111367.

(3) Abukhadra, M. R.; Allah, A. F. Synthesis and characterization of kaolinite nanotubes (KNTs) as a novel carrier for 5-fluorouracil of high encapsulation properties and controlled release. *Inorg. Chem. Commun.* **2019**, *103*, 30−36.

(4) Abukhadra, M. R.; Refay, N. M.; El-Sherbeeny, A. M.; Mostafa, A. M.; Elmeligy, M. A. Facile synthesis of bentonite/biopolymer composites as low-cost carriers for 5-fluorouracil drug; equilibrium studies and pharmacokinetic behavior. *Int. J. Biol. Macromol.* **2019**, *141*, 721−731.

(5) Yang, J.; Dai, D.; Ma, L.; Yang, Y.-W. Molecular-scale drug delivery systems loaded with oxaliplatin for supramolecular chemotherapy. *Chin. Chem. Lett.* **2021**, *32*, 729−734.

(6) Vatanparast, M.; Shariatinia, Z. AlN and AlP doped graphene quantum dots as novel drug delivery systems for 5-fluorouracil drug: theoretical studies. *J. Fluorine Chem.* **2018**, *211*, 81−93.

(7) Praphakar, R. A.; Jeyaraj, M.; Mehnath, S.; Higuchi, A.; Ponnamma, D.; Sadasivuni, K. K.; Rajan, M. A pH-sensitive guar gum-grafted-lysine-β-cyclodextrin drug carrier for the controlled release of 5-flourouracil into cancer cells. *J. Mater. Chem.* **2018**, *6*, 1519−1530.

(8) Abo-zeid, Y.; Williams, G. R. The potential anti-infective applications of metal oxide nanoparticles. *Wiley Interdiscip. Rev.: Nanomed. Nanobiotechnol.* **2020**, *12*, No. e1592.

(9) Yaneva, Z.; Ivanova, D.; Popov, N. Clinoptilolite Microparticles as Carriers of Catechin-Rich Acacia catechu Extracts: Microencapsulation and In Vitro Release Study. *Molecules* **2021**, *26*, 1655.

(10) Tan, D.; Yuan, P.; Dong, F.; He, H.; Sun, S.; Liu, Z. Selective loading of 5-fluorouracil in the interlayer space of methoxy-modified kaolinite for controlled release. *Appl. Clay Sci.* **2018**, *159*, 102−106.

(11) Abukhadra, M. R.; Refay, N. M.; El-Sherbeeny, A. M.; El-Meligy, M. A. Insight into the Loading and Release Properties of MCM-48/Biopolymer Composites as Carriers for 5-Fluorouracil: Equilibrium Modeling and Pharmacokinetic Studies. *ACS Omega* **2020**, *5*, 11745−11755.

(12) Macedo, L. D. O.; Barbosa, E. J.; Löbenberg, R.; Bou-Chacra, N. A. Anti-inflammatory drug nanocrystals: state of art and regulatory perspective. *Eur. J. Pharm. Sci.* **2021**, *158*, 105654.

(13) Lu, C.; Xiao, Y.; Liu, Y.; Sun, F.; Qiu, Y.; Mu, H.; Duan, J. Hyaluronic acid-based levofloxacin nanomicelles for nitric oxide-triggered drug delivery to treat bacterial infections. *Carbohydr. Polym.* **2020**, *229*, 115479.

(14) Khang, M. K.; Zhou, J.; Co, C. M.; Li, S.; Tang, L. A pretargeting nanoplatform for imaging and enhancing anti-inflammatory drug delivery. *Biomaterials* **2020**, *5*, 1102−1112.

(15) Sur, S.; Rathore, A.; Dave, V.; Reddy, K. R.; Chouhan, R. S.; Sadhu, V. Recent developments in functionalized polymer nanoparticles for efficient drug delivery system. *Nano-Struct. Nano-Objects* **2019**, *20*, 100397.

(16) Rahbar, M.; Morsali, A.; Bozorgmehr, M. R.; Beyramabadi, S. A. Quantum chemical studies of chitosan nanoparticles as effective drug delivery systems for 5-fluorouracil anticancer drug. *J. Mol. Liq.* **2020**, *302*, 112495.

(17) Othman, S. I.; Allam, A. A.; Al Fassam, H.; Abu-Taweel, G. M.; Altoom, N.; Abukhadra, M. R. Sonoco Green Decoration of Clinoptilolite with MgO Nanoparticles as a Potential Carrier for 5-Fluorouracil Drug: Loading Behavior, Release Profile, and Cytotoxicity. *J. Inorg. Organomet. Polym. Mater.* **2021**, 1−15.

(18) Çiftçi, H.; Arpa, M. D.; Gülaçar, İ. M.; Özcan, L.; Ersoy, B. Development and evaluation of mesoporous montmorillonite/

magnetite nanocomposites loaded with 5-Fluorouracil. *Microporous Mesoporous Mater.* **2020**, *303*, 110253.
(19) Jin, L.; Liu, Q.; Sun, Z.; Ni, X.; Wei, M. Preparation of 5-Fluorouracil/β-Cyclodextrin Complex Intercalated in Layered Double Hydroxide and the Controlled Drug Release Properties. *Ind. Eng. Chem. Res.* **2010**, *49*, 11176−11181.
(20) Tian, L.; Abukhadra, M. R.; Mohamed, A. S.; Nadeem, A.; Ahmad, S. F.; Ibrahim, K. E. Insight into the Loading and Release Properties of an Exfoliated Kaolinite/Cellulose Fiber (EXK/CF) Composite as a Carrier for Oxaliplatin Drug: Cytotoxicity and Release Kinetics. *ACS Omega* **2020**, *5*, 19165−19173.
(21) Elboughdiri, N. The use of natural zeolite to remove heavy metals Cu (II), Pb (II) and Cd (II), from industrial wastewater. *Cogent Eng.* **2020**, *7*, 1782623.
(22) Vasylechko, V. O.; Klyuchivska, O. G. Y.; Manko, N. O.; Gryshchouk, G. V.; Kalychak, Y. M.; Zhmurko, I. I.; Stoika, R. S. Novel nanocomposite materials of silver-exchanged clinoptilolite with pre-concentration of Ag(NH3)2+ in water possess enhanced anticancer action. *Appl. Nanosci.* **2020**, *10*, 4869−4878.
(23) Servatan, M.; Zarrintaj, P.; Mahmodi, G.; Kim, S.-J.; Ganjali, M. R.; Saeb, M. R.; Mozafari, M. Zeolites in drug delivery: Progress, challenges and opportunities. *Drug Discovery Today* **2020**, *25*, 642−656.
(24) Sandomierski, M.; Buchwald, Z.; Koczorowski, W.; Voelkel, A. Calcium forms of zeolites A and X as fillers in dental restorative materials with remineralizing potential. *Microporous Mesoporous Mater.* **2020**, *294*, 109899.
(25) Kraljević Pavelić, S.; Simović Medica, J.; Gumbarević, D.; Filošević, A.; Pržulj, N.; Pavelić, K. Critical review on zeolite clinoptilolite safety and medical applications in vivo. *Front. Pharmacol.* **2018**, *9*, 1350.
(26) Vargas, A. M.; Cipagauta-Ardila, C. C.; Molina-Velasco, D. R.; Ríos-Reyes, C. A. Surfactant-modified natural zeolites as carriers for diclofenac sodium release: A preliminary feasibility study for pharmaceutical applications. *Mater. Chem. Phys.* **2020**, *256*, 123644.
(27) Souza, I. M. S.; Sainz-Díaz, C. I.; Viseras, C.; Pergher, S. B. C. Adsorption capacity evaluation of zeolites as carrier of isoniazid. *Microporous Mesoporous Mater.* **2020**, *292*, 109733.
(28) Mostafa, M.; El-Meligy, M. A.; Sharaf, M.; Soliman, A. T.; AbuKhadra, M. R. Insight into chitosan/zeolite-A nanocomposite as an advanced carrier for levofloxacin and its anti-inflammatory properties; loading, release, and anti-inflammatory studies. *Int. J. Biol. Macromol.* **2021**, *179*, 206−216.
(29) Som, A.; Raliya, R.; Paranandi, K.; High, R. A.; Reed, N.; Beeman, S. C.; Brandenburg, M.; Sudlow, G.; Prior, J. L.; Akers, W.; Mah-Som, A. Y. Calcium carbonate nanoparticles stimulate tumor metabolic reprogramming and modulate tumor metastasis. *Nanomedicine* **2019**, *14*, 169−182.
(30) Maringgal, B.; Hashim, N.; Tawakkal, I. S. M. A.; Hamzah, M. H.; Mohamed, M. T. M. Biosynthesis of CaO nanoparticles using Trigona sp. Honey: Physicochemical characterization, antifungal activity, and cytotoxicity properties. *J. Mater. Res. Technol.* **2020**, *9*, 11756−11768.
(31) Rabie, A. M.; Shaban, M.; Abukhadra, M. R.; Hosny, R.; Ahmed, S. A.; Negm, N. A. Diatomite supported by CaO/MgO nanocomposite as heterogeneous catalyst for biodiesel production from waste cooking oil. *J. Mol. Liq.* **2019**, *279*, 224−231.
(32) Toledo Arana, J.; Torres, J. J.; Acevedo, D. F.; Illanes, C. O.; Ochoa, N. A.; Pagliero, C. L. One-step synthesis of CaO-ZnO efficient catalyst for biodiesel production. *Int. J. Chem. Eng.* **2019**, *2019*, 1806017.
(33) Salam, M. A.; AbuKhadra, M. R.; Mohamed, A. S. Effective oxidation of methyl parathion pesticide in water over recycled glass based-MCM-41 decorated by green Co_3O_4 nanoparticles. *Environ. Pollut.* **2020**, *259*, 113874.
(34) Shaban, M.; Abukhadra, M. R. Geochemical evaluation and environmental application of Yemeni natural zeolite as sorbent for Cd^{2+} from solution: kinetic modeling, equilibrium studies, and statistical optimization. *Environ. Earth Sci.* **2017**, *76*, 310.
(35) Mansouri, N.; Rikhtegar, N.; Panahi, H. A.; Atabi, F.; Shahraki, B. K. Porosity, characterization and structural properties of natural zeolite-clinoptilolite-as a sorbent. *Environ. Prot. Eng.* **2013**, *39*, 139−152.
(36) Shaban, M.; Sayed, M. I.; Shahien, M. G.; Abukhadra, M. R.; Ahmed, Z. M. Adsorption behavior of inorganic-and organic-modified kaolinite for Congo red dye from water, kinetic modeling, and equilibrium studies. *J. Sol-Gel Sci. Technol.* **2018**, *87*, 427−441.
(37) Safwat, M. A.; Soliman, G. M.; Sayed, D.; Attia, M. A. Gold nanoparticles enhance 5-fluorouracil anticancer efficacy against colorectal cancer cells. *Int. J. Pharm.* **2016**, *513*, 648−658.
(38) Abukhadra, M. R.; Ibrahim, S. M.; Ashraf, M. T.; Khim, J. S.; Allam, A. A.; Ajarem, J. S.; Mahmoud, H. S. Insight into β-cyclodextrin/diatomite hybrid structure as a potential carrier for ibuprofen drug molecules; equilibrium, release properties, and cytotoxicity. *J. Sol. Gel Sci. Technol.* **2021**, *100*, 101−114.
(39) Luo, H.; Ji, D.; Li, C.; Zhu, Y.; Xiong, G.; Wan, Y. Layered nanohydroxyapatite as a novel nanocarrier for controlled delivery of 5-fluorouracil. *Int. J. Pharm.* **2016**, *513*, 17−25.
(40) Li, Z.; Zhang, B.; Jia, S.; Ma, M.; Hao, J. Novel supramolecular organogel based on β-cyclodextrin as a green drug carrier for enhancing anticancer effects. *J. Mol. Liq.* **2018**, *250*, 19−25.
(41) Liu, Y.; Yan, C.; Zhao, J.; Zhang, Z.; Wang, H.; Zhou, S.; Wu, L. Synthesis of zeolite P1 from fly ash under solvent-free conditions for ammonium removal from water. *J. Clean. Prod.* **2018**, *202*, 11−22.
(42) Goscianska, J.; Olejnik, A.; Nowak, I.; Marciniak, M.; Pietrzak, R. Ordered mesoporous silica modified with lanthanum for ibuprofen loading and release behaviour. *Eur. J. Pharm. Biopharm.* **2015**, *94*, 550−558.
(43) Rehman, F.; Ahmed, K.; Rahim, A.; Muhammad, N.; Tariq, S.; Azhar, U.; Khan, A. J.; Sama, Z.; Volpe, P. L.; Airoldi, C. Organo-bridged silsesquioxane incorporated mesoporous silica as a carrier for the controlled delivery of ibuprofen and fluorouracil. *J. Mol. Liq.* **2018**, *258*, 319−326.
(44) Sun, L.; Chen, Y.; Zhou, Y.; Guo, D.; Fan, Y.; Guo, F.; Zheng, Y.; Chen, W. Preparation of 5-fluorouracil-loaded chitosan nanoparticles and study of the sustained release in vitro and in vivo. *Asian J. Pharm. Sci.* **2017**, *12*, 418−423.
(45) Gouda, R.; Baishya, H.; Qing, Z. Application of mathematical models in drug release kinetics of carbidopa and levodopa ER tablets. *J. Dev. Drugs* **2017**, *6*, 1000171.
(46) Lin, F. H.; Lee, Y. H.; Jian, C. H.; Wong, J. M.; Shieh, M. J.; Wang, C. Y. A study of purified montmorillonite intercalated with 5-fluorouracil as drug carrier. *Biomaterials* **2002**, *23*, 1981−1987.
(47) Datt, A.; Burns, E. A.; Dhuna, N. A.; Larsen, S. C. Loading and release of 5-fluorouracil from HY zeolites with varying SiO_2/Al_2O_3 ratios. *Microporous Mesoporous Mater.* **2013**, *167*, 182−187.
(48) Ge, M.; Tang, W.; Du, M.; Liang, G.; Hu, G.; Alam, S. J. Research on 5-fluorouracil as a drug carrier materials with its in vitro release properties on organic modified magadiite. *Eur. J. Pharm. Sci.* **2019**, *130*, 44−53.
(49) Wang, G.; Lu, X.; Qiu, J.; Chen, P.; Chinese, J. Preparation and release performance of fluorouracil/montmorillonite complexes. *J. Chin. Ceram. Soc.* **2010**, *38*, 678−683.

https://doi.org/10.1021/acsomega.1c04725
ACS Omega 2021, 6, 31982−31992